



## Corrosion behavior of novel Cu–Ni–Al–Si alloy with super-high strength in 3.5% NaCl solution

Jia-jun ZHU<sup>1,2</sup>, San-hua LI<sup>3</sup>, Lei-nuo SHEN<sup>3</sup>, Wu-lin YANG<sup>1,2</sup>, Zhou LI<sup>3</sup>

1. College of Materials Science and Engineering, Hunan University, Changsha 410082, China;

2. Hunan Province Key Laboratory for Spray Deposition Technology and Application, Hunan University, Changsha 410082, China;

3. School of Materials Science and Engineering, Central South University, Changsha 410083, China

Received 21 March 2016; accepted 1 September 2016

**Abstract:** A novel Cu–6.5Ni–1Al–1Si–0.15Mg–0.15Ce alloy with super-high strength was designed and its corrosion behavior in 3.5% NaCl solution at 25 °C was investigated by the means of SEM observation, TEM observation and XPS analysis. The alloy after solution treatment, 80% cold rolling and aging at 450 °C for 1 h had the best comprehensive properties with hardness of HV 314, electrical conductivity of 19.4% IACS, tensile strength of 1017 MPa, and average annual corrosion rate of 0.028 mm/a. The oxides and chloride products formed at first, followed by the formation of dyroxides products. The alloy showed super-high strength, good electrical conductivity and corrosion resistant because Ni<sub>2</sub>Si hindered the precipitation of large NiAl at the grain boundary and the denickelification of the alloy.

**Key words:** Cu–Ni–Al–Si alloy; Ni<sub>2</sub>Si precipitate; corrosion behavior; average annual corrosion rate; corrosion product

### 1 Introduction

The super-high strength elastic copper alloys have been widely used as hull, electrical wires, springs, pipes, valves, condensers, heat exchangers and propeller in marine engineering fields [1,2]. These copper alloys not only present relatively high strength and hardness, good electrical conductivity, thermal conductivity and stress relax resistant, but also have excellent corrosion resistant and good performance to prevent the growth and adhesion of marine organisms [3,4]. In particular, Cu–Be alloys exhibit the best comprehensive properties among those copper alloys. However, the element Be forms beryllium oxide during melting and processing processes, which is harmful to health. Besides, the stress relax rate of Cu–Be alloys increases to 25% when work temperature is over 150 °C, which limits their application at high temperature.

Cu–Ni–Sn, Cu–Ni–Mn and Cu–Ti alloys have been developed to substitute the toxic Cu–Be alloys. ROH et al [5] reported that Cu–5Ni–10Sn alloy had a maximum tensile strength of 1165 MPa, and subsequent

aging treatment slightly reduced the tensile strength to 1000–1100 MPa. RHU et al [6] found that the ultimate tensile strength of Cu–6Ni–2Mn–2Sn–2Al alloy was 950 MPa after cold rolling by 80%. LI et al [7] indicated that the tensile strength and yield strength of Cu–2.7Ti–0.15Mg–0.1Ce–0.1Zr alloy reached up to 1035 MPa and 982 MPa, respectively. However, those alloys suffered from localized corrosion due to the selective corrosion of Ni or Ti in both fresh and sea water [8]. In recent years, Cu–Ni–Al alloys have attracted a lot of interests due to their high strength and good corrosion resistant. CHO et al [9] reported that Cu–6.97Ni–2.91Al alloy reached up to HV 2620 after cold rolling by 77% and aging at 500 °C for 1.0×10<sup>4</sup> s, and the high hardness of the Cu–Ni–Al alloy was attributed to the precipitation of NiAl and Ni<sub>3</sub>Al. The addition of Al elements improved the corrosion resistant of Cu–Ni–Al alloys because the Al<sub>2</sub>O<sub>3</sub> corrosion product condensed the porous layer of Cu<sub>2</sub>O and produced a protective oxide product film, which decreased the electrochemical reaction rate and hindered the denickelification [10]. However, the electrical conductivity Cu–Ni–Al alloys was lower than 15% IACS. LEI et al [11] and LI et al [12] found that the

addition of silicon formed  $\text{Ni}_2\text{Si}$  particles during aging, which would strongly hinder the movement of dislocations and improve the strength. In order to maintain the strength and further improve the electrical conductivity and corrosion resistant of Cu–Ni–Al alloy, the element Si was added in Cu–Ni–Al alloy in our study and Cu–6.5Ni–1Al–1Si–0.15Mg–0.15Ce alloy was designed. In this work, the influence of aging on comprehensive properties and microstructure of the designed Cu–Ni–Al–Si alloy was investigated. The corrosion behavior and corrosion mechanism of the designed Cu–Ni–Al–Si alloy were discussed. The comprehensive properties of the designed Cu–Ni–Al–Si alloy were compared with the traditional Cu–Ni–Al alloy.

## 2 Experimental

### 2.1 Material preparation

The pure Cu, Ni, Al, Si, Cu–Ce and Cu–Mg intermediate alloys were melted in the induction furnace. The Cu–Ce and Cu–Mg intermediate alloys were added in order to avoid the melting loss of pure Ce and Mg. The Cu–6.5Ni–1Al–1Si–0.15Ce–0.15Mg (mass fraction, %) alloy was prepared by casting method. The as-cast alloy was hot-rolled by 60% at 920 °C, solution-treated at 960 °C for 4 h, cold-rolled by 80%, and then aged at 450 °C in a salt bath of  $\text{KNO}_3$  and  $\text{NaNO}_3$  solution.

### 2.2 Mechanical tests and electrical conductivity tests

The hardness tests were conducted on a Vicker's hardness tester, with a holding time of 10 s, and a load of 2 kg. The tensile tests were performed on an Instron 8019 tester at 20 °C with a constant strain rate of  $1.0 \times 10^{-2}$  mm/s. Electrical conductivity was measured using a double-arm electrical bridge device.

### 2.3 Average annual corrosion rate tests

The aged plates were cut into samples with dimensions of 30 mm × 30 mm, and each sample was weighed on an AEL–200 electronic analytical balance. Then, part of samples were exposed in 3.5% NaCl solution at 25 °C for 720 h, then immersed in 1:1 HCl water solution for 15 min to remove the corrosion products on the surfaces, and finally weighed. The mass loss of samples exposed for 720 h ( $\Delta m$ ) was calculated (including the mass loss caused by corrosion in NaCl solution and reaction with HCl solution). The other samples without being exposed in 3.5% NaCl solution were immersed in 1:1 HCl water solution for 15 min to calculate the mass loss caused by reaction with HCl solution. The average annual corrosion rate was calculated as follows [13]:

$$R = 8.76 \times 10^7 \frac{\Delta m - \Delta m_k}{St\rho} \quad (1)$$

where  $R$  is the immersion corrosion rate per year,  $S$  is the total surface area,  $t$  is the immersion time,  $\rho$  is the density of samples,  $\Delta m$  is the mass loss of samples after being exposed for 720 h,  $\Delta m_k$  is the mass loss of samples without exposed in NaCl.

### 2.4 Electrochemical tests

The plate was cut into the samples with the sizes of 10 mm × 10 mm × 1.5 mm. Each sample had one copper wire welded on the surface, sealed with a denture powder, and then exposed in 3.5% NaCl solution at 25 °C for different time. The electrochemical tests were conducted on an IM6EX electrochemical workstation, using Pt as the auxiliary electrode and the saturated calomel electrode (SCE) as the reference electrode. The voltage of polarization tests was from –300 to 600 mV with a scanning rate of 2 mV/s. The frequency of electrochemical impedance spectroscopy (EIS) tests was from 10 mHz to 100 kHz, with amplitude of 20 mV.

### 2.5 Microstructure analysis

Transmission electron microscopy (TEM) and selected area diffraction pattern (SADP) observations were performed on a JEM–2100F, with the operation voltage of 200 kV. The specimens for TEM observations were mechanically reduced to 0.06 mm and then electron-polished by the standard twin-jet electro-polishing method using the methanol–nitric acid solution with a volume ratio of 3:1 at a temperature between –20 °C and –30 °C. The scanning electron microscopy (SEM) observation and energy dispersive X-ray spectroscopy (EDX) analysis were conducted on a Sirion 200 scanning electron microscope. X-ray photoelectron spectroscopy (XPS) analysis of exposed samples was conducted on a  $\text{K}_\alpha$  1063 X-ray photoelectron spectroscope with a monochromatized Al K X-ray source in a vacuum of  $1.0 \times 10^{-7}$  Pa. The scanning step was 1 eV for wide scanning and 0.1 eV for narrow scanning.

## 3 Results and discussion

### 3.1 Mechanical properties and electrical conductivity

Figure 1 showed the variation of hardness and electrical conductivity of the designed Cu–6.5Ni–1Al–1Si–0.15Ce–0.15Mg alloy after solution treatment, cold rolling by 80% and then aging at 450 °C for different time. The electrical conductivity increased with aging time. The hardness increased sharply at the initial stage of aging and reached its peak value after aging for 15 min. As aging time further increased, the hardness gradually decreased.

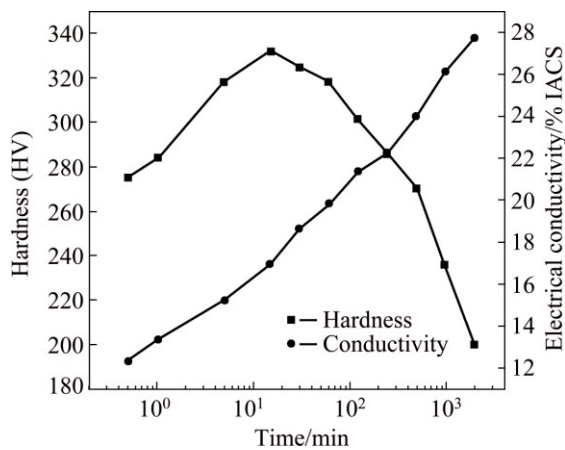


Fig. 1 Hardness and electrical conductivity curves of alloy

The cold rolling introduced a great number of dislocations in the alloy. Recovery and precipitation occurred during aging, which decreased the amount of solid soluted atoms, resulting in the increase of electrical conductivity. At early stage of aging, a plenty of nano-scale precipitates nucleated in the matrix, which interacted with dislocations and hindered the movement of dislocations, leading to the increase of strength; further increasing aging time, recovery was accelerated and precipitates coarsened, resulting in the decrease of strength [14].

Considering the combination of hardness and electrical conductivity, three different thermomechanical treatments were chosen to conduct the tensile tests. The results indicated that tensile strength and yield strength decreased, while elongation increased with the increase of aging time, as shown in Table 1. The sample after being cold-rolled by 80% and then aged at 450 °C for 1 h had the best comprehensive properties with hardness of HV 314, electrical conductivity of 19.4%IACS, tensile strength of 1017 MPa, yield strength of 1002 MPa and elongation of 2.5%.

### 3.2 Microstructure observation

Figure 2 showed the bright field micrographs and corresponding SADPs of the solution-treated alloy after cold rolling by 80% and then aging at 450 °C for different time. After aging at 450 °C for 15 min, two kinds of nano-scale particles, i.e., the globe particles with size of about 5 nm and rod-shape particles with size of

about 8 nm precipitated in the matrix (Fig. 2(a)). The corresponding SADP indicated that those globe particles were  $\text{Ni}_3\text{Al}$ , while the rod-shape particles were  $\delta\text{-Ni}_2\text{Si}$ , which had two variants perpendicular with each other (Fig. 2(b)). Increasing aging time to 1 h, both  $\text{Ni}_3\text{Al}$  with size of 20 nm and  $\delta\text{-Ni}_2\text{Si}$  with size of 30 nm precipitated (Figs. 2(c) and (d)). Compared with the alloy aged for 15 min, the volume fraction of those precipitates increased in the alloy aged for 1 h. As the alloy aged at 450 °C for 4 h, the sizes of  $\delta\text{-Ni}_2\text{Si}$  and  $\text{Ni}_3\text{Al}$  particles were 80 nm and 50 nm, respectively, indicating that those precipitates coarsened rapidly with aging time further prolonging (Figs. 2(e) and (f)).

### 3.3 Corrosion resistant

The sample with the best comprehensive properties (ST+80% CR+450 °C, 1 h) was selected to conduct the corrosion tests. The measured annual average corrosion rate of the sample was 0.028 mm/a. Figure 3 showed the polarization curves of the samples after being exposed for different time. An active–passive transition followed by a short passive region was observed in the anodic curve of the sample exposed for less than 16 d. When the samples was immersed for over 16 d, the current density increased sharply at a definite potential in anodic curves, due to the breakdown of passivity and formation of pitting [15]. The pitting potential increased as exposure time prolonged to 30 d, indicating the increase of pitting resistant.

The anode Tafel slope ( $b_a$ ), cathode Tafel slope ( $b_c$ ) and corrosion current density ( $J_{\text{corr}}$ ) can be obtained by fitting the polarization curves, therefore, the polarization resistant ( $R_p$ ) can be calculated by the following equation [16]:

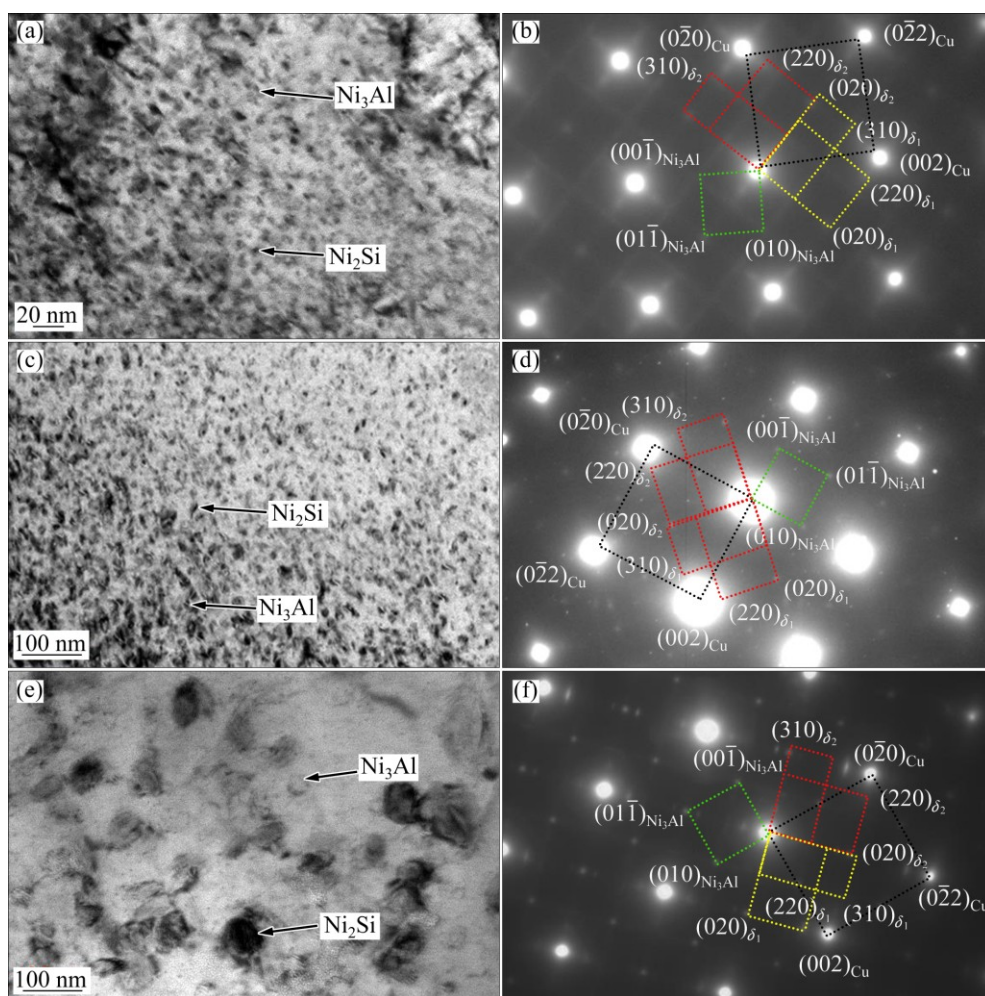
$$R_p = \frac{b_a \times |b_c|}{2.303(b_a \times |b_c|) \times J_{\text{corr}}} \quad (2)$$

The parameters of polarization curves were shown in Table 2. The calculated results showed that the polarization resistant increased with exposure time, indicating the condense of corrosion products and the increase of corrosion resistant.

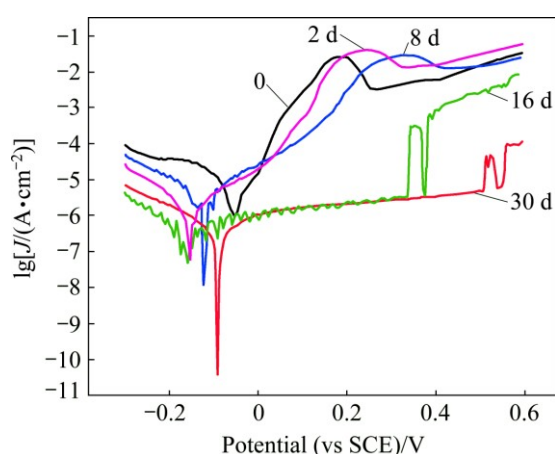
The Nyquist plots of the samples exposed in NaCl solution for different time were shown in Fig. 4. The Nyquist plots were typical semicircle ones. The diameter of the semicircle increased with the increase of exposure

Table 1 Comprehensive properties of alloy after aging at 450 °C for different time

Thermomechanical treatment	Hardness (HV)	Electrical conductivity /% IACS	Tensile strength/ MPa	Yield strength/ MPa	Elongation/ %
ST+80% CR+450 °C, 15 min	332	16.9	1032	1011	2.4
ST+80% CR+450 °C, 1 h	314	19.4	1017	1002	2.5
ST+80% CR+450 °C, 4 h	285	22.2	922	901	2.6



**Fig. 2** Bright-field micrographs and SADPs of solution-treated alloy after cold rolling by 80% and aging at 450 °C for different time: (a) Bright-field micrograph, aged for 15 min; (b) SADP of (a); (c) Bright-field micrograph, aged for 1 h; (d) SADP of (c); (e) Bright-field micrograph, aged for 4 h; (f) SADP of (e)



**Fig. 3** Polarization curves of alloy after being exposed in NaCl solution for different time

time, due to the condense of corrosion product film. In order to further analyze the Nyquist plots, the equivalent circuit model was applied to fitting those curves [17]. The equivalent circuit model was shown in Fig. 5 and the fitted parameters were shown in Table 3. The capacitance

of corrosion product film ( $C_f$ ) and the coefficient of CPE (CPE-T) decreased with exposure time, while the resistance of corrosion product film ( $R_f$ ), the transfer resistance ( $R_c$ ) and Warburg impedance increased with exposure time, indicating that the corrosion product film became thicker and denser with the increase of exposure time.

### 3.4 Corrosion product analysis

Figure 6 presented the microstructure of the surfaces of the samples after being exposed in 3.5% NaCl solution for 1 h, 2 d and 30 d. When the sample was exposed for 1 h, a plenty of corrosion products began to form on the surface, as shown in Figs. 6(a) and 6(b). The corresponding EDX analysis of Fig. 6(b) showed that Cu, Ni, Al and Si, O and Cl elements were detected on the surface of the sample, while the peak of O was much stronger than that of Cl, suggesting that oxide was the main corrosion products at the early stage of corrosion (Fig. 6(g)). Increasing exposure time to 2 d, a uniform oxide product film formed on the surface of

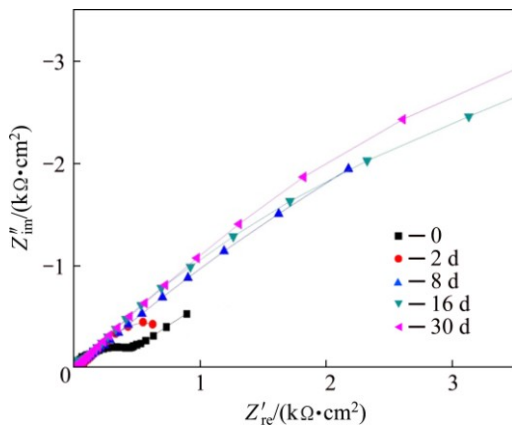
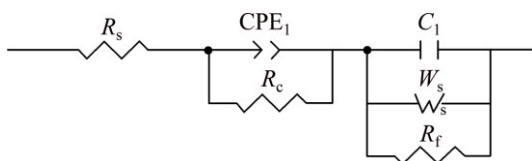
**Table 2** Parameters of polarization curves of samples after ST+80% CR+ 450 °C, 1 h treatment

Exposure time/d	$b_c/$ (mV·Dec <sup>-1</sup> )	$b_a/$ (mV·Dec <sup>-1</sup> )	$\phi_{\text{corr}}/$ mV	$J_{\text{corr}}/$ (10 <sup>-6</sup> A·cm <sup>-2</sup> )	$R_p/$ (kΩ·cm <sup>2</sup> )
0	-123	68.5	-54.5	17.75	1.08
2	-131	90.1	-151.5	1.83	12.67
8	-143	105.3	-109.4	1.01	26.07
16	-163	156.2	-164.3	0.36	96.21
30	-187	190.0	-75.98	0.40	102.30

**Table 3** Calculated parameters of Nyquist plots of samples exposed for different time

Exposed time/d	$R_s/$ (Ω·cm <sup>2</sup> )	CPE-T	CPE-P	$R_c/$ (Ω·cm <sup>2</sup> )	$C_f/$ (μF·cm <sup>-2</sup> )	$W_s\text{-R}$	$W_s\text{-T}$	$W_s\text{-P}$	$R_f/$ (Ω·cm <sup>2</sup> )
0	5.30	0.000870	0.528	12656	0.821	2.098	2.498×10 <sup>-6</sup>	0.264	101.4
2	6.14	0.000670	0.562	12882	0.758	3.476	1.731×10 <sup>-5</sup>	0.281	145.5
8	34.76	0.000104	0.573	23180	0.718	4.132	7.556×10 <sup>-2</sup>	0.283	2318.0
16	35.62	0.000101	0.579	23535	0.716	4.151	7.574	0.284	2417.2
30	45.44	0.000028	0.589	73535	0.658	4.252	7.893	0.285	3180.6

CPE-P: Fitting capacitance coefficient of corrosion product film;  $W_s\text{-R}$ ,  $W_s\text{-T}$  and  $W_s\text{-P}$ : Fitting coefficients of Warburg impedance;  $R_s$ : Solution resistance

**Fig. 4** Nyquist plots of alloy after being exposed in NaCl solution for different time**Fig. 5** Equivalent circuit model used to fit Nyquist plots ( $R_s$ —Solution resistance;  $C_f$ —Capacitance of film;  $R_c$ —Charge transfer resistance; CPE—Constant phase element;  $W_s$ —Finite Warburg element;  $R_f$ —Resistance of film)

the sample and chloride corrosion product aggregated on part of the oxide product film (Figs. 6(c) and (d)). The EDX analysis of Fig. 6(d) showed that the intensity of the peaks of Cl and O increased sharply, indicating the increase of the amount of oxide and chloride corrosion products (Fig. 6(h)). The amount of chloride corrosion products increased as exposure time further increased to 30 d, and a double-layer corrosion film with an inner layer of oxide products and an outer layer of chloride

product formed (Figs. 6(e) and (f)).

The wide XPS spectra of the samples exposed in 3.5% NaCl solution for 1 h and 30 d were shown in Fig. 7. The main peaks of Cu, O, Cl and Al elements were detected in both samples, indicating that the main corrosion products in both samples were oxide and chloride products of Cu and Al. The intensity of the peaks of Cu decreased, while that of O and Cl increased as exposure time increased, suggesting the thickening of corrosion products.

The narrow XPS spectra of Cu, O and Cl of the samples exposed for 1 h and 30 d were shown in Fig. 8. When the sample was exposed for 1 h, the corrosion products of Cu existed in the forms of CuCl, CuCl<sub>2</sub>, Cu<sub>2</sub>O and CuO, while CuCl and CuO were the main products (Fig. 8(a)). The peaks of CuO, Cu<sub>2</sub>O, Al<sub>2</sub>O<sub>3</sub> and Cu(OH)<sub>2</sub> were observed in the narrow spectra of O (Fig. 8(c)). The chloride products were CuCl and CuCl<sub>2</sub> (Fig. 8(e)). With increasing exposure time to 30 d, the amount of CuCl<sub>2</sub>, CuO, and Cu(OH)<sub>2</sub> increased, while that of Cu<sub>2</sub>O and CuCl decreased (Figs. 8(b), (d) and (f)). These results indicated that oxides formed at the initial stage of corrosion, and those oxides were further oxidized, hydroxidized and chloridized as exposure time increased.

### 3.5 Corrosion behavior and mechanism

The corrosion behavior of the designed Cu–6.5Ni–1Al–1Si–0.15Mg–0.15Ce alloy was relative to its composition and microstructure. After solution treatment, cold rolling and then aging at 450 °C, the super saturated solid solution of the alloy decomposed and secondary phase precipitated. When the aged alloy was immersed in

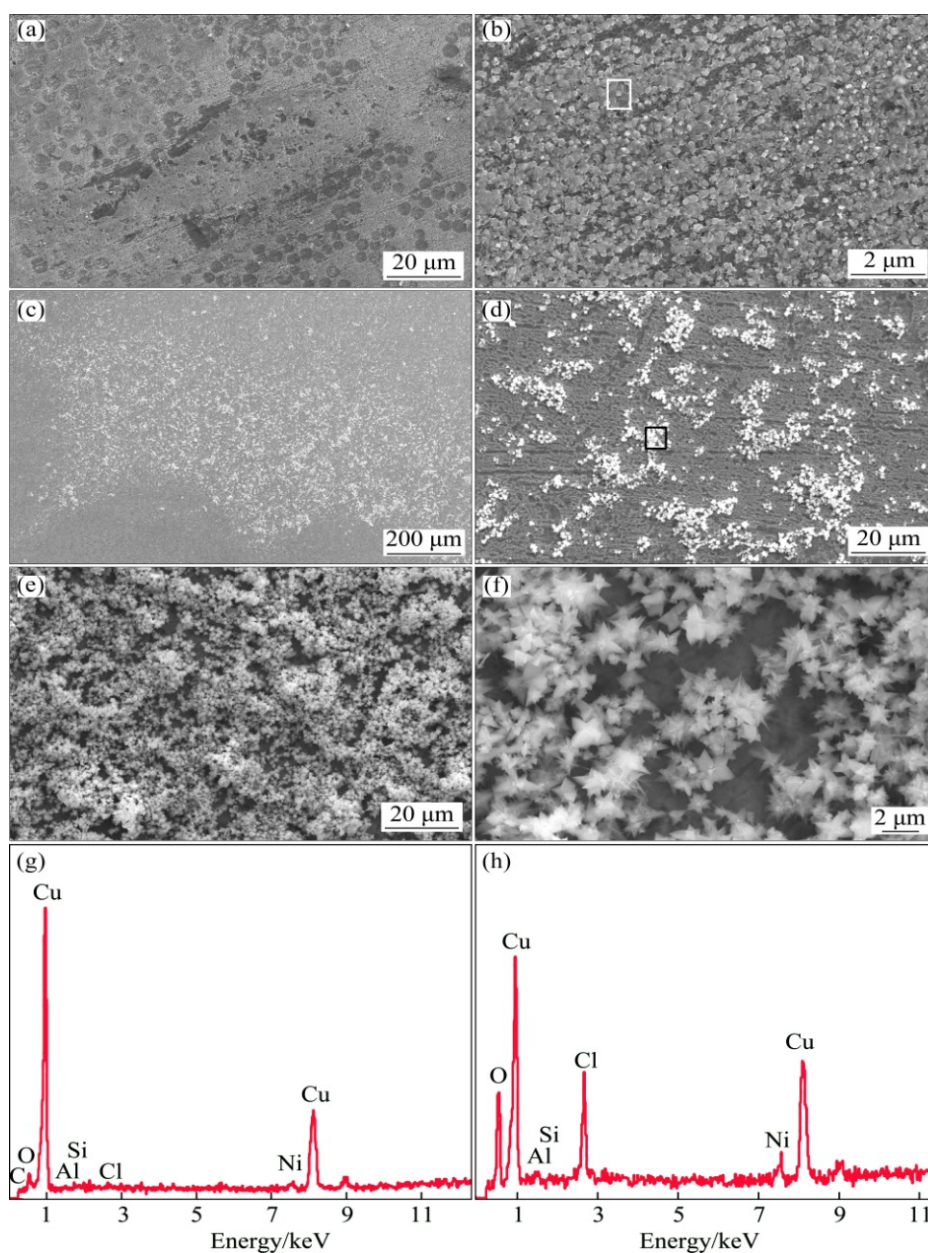


**Fig. 6** Microstructures of alloy surface and EDX analysis of corrosion products after being exposed in NaCl solution for different time: (a, b) 1 h; (c, d) 2 d; (e, f) 30 d; (g) EDX of corrosion product of (b); (h) EDX of corrosion product of (d)

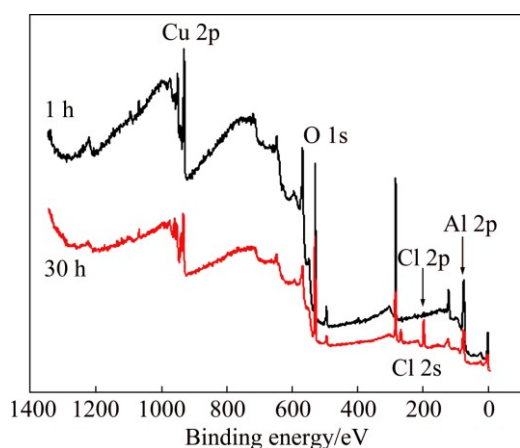


**Fig. 7** Wide XPS spectra of samples exposed for 1 h and 30 d

3.5% NaCl solution, the metallic elements such as Cu, Al and Ni acted as anode, while those secondary phases acted as cathode. The courses of anodic dissolution can be described as [18,19]



The cathodic reaction can be described as



Those metallic ions and chlorides would be hydrolyzed and formed dioxides or oxides [20,21].

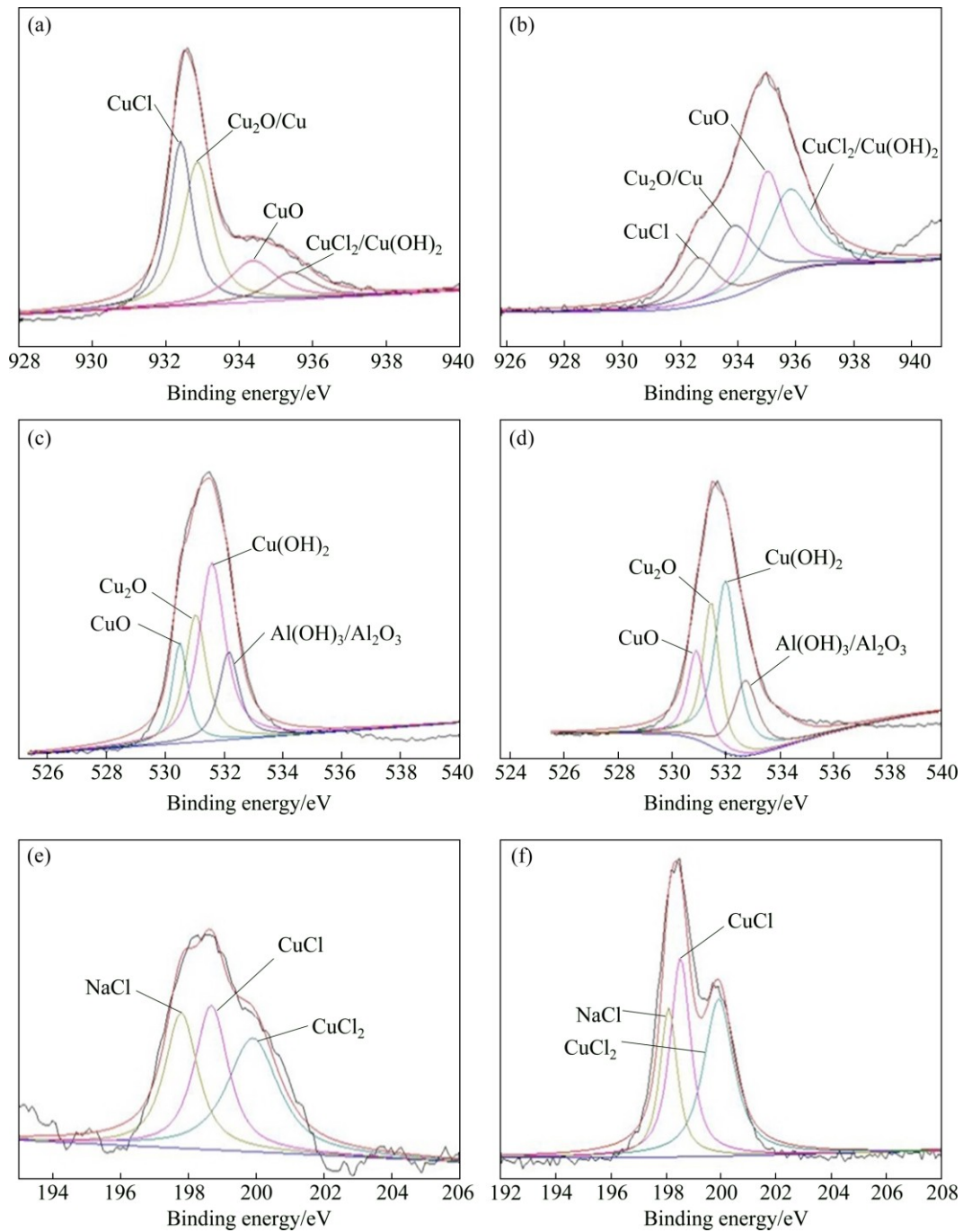
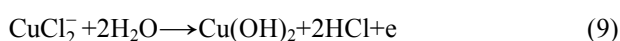
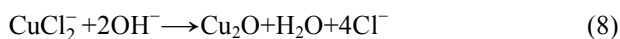


**Fig. 8** Narrow XPS spectra of samples exposed for different time: (a) 24 h, Cu; (b) 30 d, Cu; (c) 24 h, O; (d) 30 d, O; (e) 24 h, Cl; (f) 30 d, Cl



As immersing time increased, the corrosion products film condensed and thickened as immersion

time increased, leading to the increase of corrosion resistant. The above analyses indicated that Cu, Al, Ni chlorides, oxides and dyoxides were able to form during corrosion. However, only  $\text{Cu}_2\text{O}$ ,  $\text{CuO}$ ,  $\text{CuCl}$ ,  $\text{CuCl}_2/\text{Cu}(\text{OH})_2$ , and  $\text{Al}_2\text{O}_3/\text{Al}(\text{OH})_3$  were observed in the designed Cu-6.5Ni-1Al-1Si-0.15Mg-0.15Ce alloy.

The corrosion resistant of copper alloys can be attributed to a protective layer consisting mainly of the thin and strongly adherent inner barrier  $\text{Cu}_2\text{O}$  layer. However, those traditional Cu-Ni-X alloys suffered

from the selective corrosion of nickel [22]. The addition of Al elements improved the corrosion resistant of the designed alloys because the  $\text{Al}_2\text{O}_3$  corrosion product condensed the porous layer of  $\text{Cu}_2\text{O}$  and produced a protective oxide product film, which would decrease the electrochemical reaction rate and hinder the denickelification [10]. In the designed Cu–6.5Ni–1Al–1Si–0.15Mg–0.15Ce alloy, the addition of silicon formed  $\text{Ni}_2\text{Si}$  particles during aging, which purified the matrix and hindered the precipitation of coarsen NiAl particles at the grain boundary [23,24]. Those nano-scale  $\text{Ni}_2\text{Si}$  particles also strongly hindered the movement of dislocations and improved its strength. As a result, the designed alloy presented higher strength and electrical conductivity than the Cu–6.97Ni–2.91Al alloy. Besides, the precipitation of  $\text{Ni}_2\text{Si}$  precipitates decreased the concentration of nickel in solid solution, which significantly decreased the selective corrosion rate of nickel in the designed alloy. Therefore, the Cu–6.5Ni–1Al–1Si–0.15Mg–0.15Ce alloy presented better mechanical properties and corrosion resistant than the Cu–6.97Ni–2.91Al alloy and was able to replace the toxic Cu–Be alloy in ocean industry and many other marine engineering fields.

## 4 Conclusions

1) After solution treatment, cold rolling by 80% and then aging at 450 °C for 1 h, the designed Cu–6.5Ni–1Al–1Si–0.15Mg–0.15Ce alloy had excellent comprehensive properties with hardness of HV 314, electrical conductivity of 19.4%IACS, tensile strength of 1017 MPa, yield strength of 1002 MPa, elongation of 2.5% and average annual corrosion rate of 0.028 mm/a. Both  $\text{Ni}_3\text{Al}$  and  $\text{Ni}_2\text{Si}$  particles precipitated in the grain, and these particles coarsened as aging time prolonged.

2) The corrosion products film mainly consisted of  $\text{Cu}_2\text{O}$ , CuO, CuCl,  $\text{CuCl}_2/\text{Cu}(\text{OH})_2$ , and  $\text{Al}_2\text{O}_3/\text{Al}(\text{OH})_3$ . The polarization resistance, the resistance of the corrosion product film and the corrosion resistant of the designed alloy increased with exposure time, due to the densification and thickening of corrosion products film.

3) The designed alloy showed excellent corrosion resistant because the porous layer of  $\text{Cu}_2\text{O}$  was densified by the formation of  $\text{Al}_2\text{O}_3$  corrosion product.  $\text{Ni}_3\text{Al}$  and  $\delta\text{-Ni}_2\text{Si}$  precipitates decreased the amount of Ni in solid solution, which decreased the electrochemical reaction rate and hindered the denickelification.

## References

[1] PAN Zhi-yong, WANG Ming-pu, LI Zhou, XIAO Zhu, CHEN Chang. Thermomechanical treatment of super high strength Cu–8.0Ni–1.8Si alloy [J]. Transactions of Nonferrous Metals Society of China, 2007, 17(s1): 1076–1080.

[2] LEI Qian, LI Zhou, XIAO Tao, PANG Yong, XIANG Zi-qi, QIU Wen-ting, XIAO Zhu. A new ultrahigh strength Cu–Ni–Si alloy [J]. Intermetallics, 2013, 42: 77–84.

[3] DONG Qi-yi, SHEN Lei-nuo, WANG Ming-pu, JIA Yan-lin, LI Zhou, CAO Feng, CHEN Chang. Microstructure and properties of Cu–2.3Fe–0.03P alloy during thermomechanical treatments [J]. Transactions of Nonferrous Metals Society of China, 2015, 25(5): 1551–1558.

[4] YUAN S J, PEHKONEN S O. Surface characterization and corrosion behavior of 70/30 Cu–Ni alloy in pristine and sulfide-containing simulated seawater [J]. Corrosion Science, 2007, 49(3): 1276–1304.

[5] ROH D G, KANG H S, BAIK K H. Microstructure feature and aging characteristics of spray-formed Cu–5Ni–10Sn alloy [J]. Journal of Korean Powder Metallurgy Institute, 2012, 19(4): 317–321.

[6] RHU J C, KIM S S, HAN S Z, JUNG Y C, KIM C J. Mechanical properties of Cu–6Ni–2Mn–2Sn–xAl alloys [J]. Scripta Materialia, 2000, 42: 83–89.

[7] LI Si, LI Zhou, XIAO Zhu, LI San-hua, SHEN Lei-nuo, DONG Qi-yi. Microstructure and property of Cu–2.7Ti–0.15Mg–0.1Ce–0.1Zr alloy treated with a combined aging process [J]. Materials Science and Engineering A, 2016, 650: 345–353.

[8] JEON W S, SHUR C C, KIM J G, HAN S Z, KIM Y S. Effect of Cr on the corrosion resistance of Cu–6Ni–4Sn alloys [J]. Journal of Alloys and Compounds, 2008, 455: 358–363.

[9] CHO Y R, KIM Y H, LEE T D. Precipitation hardening and recrystallization in Cu–4% to 7%Ni–3%Al alloys [J]. Journal of Materials Science, 1991, 26: 2879–2886.

[10] SCHÜSSLER A, EXNER H E. The corrosion of nickel-aluminium bronzes in seawater-II. The corrosion mechanism in the presence of sulphide pollution [J]. Corrosion Science 1993, 34: 1803–1815.

[11] LEI Q, LI Z, DAI C, WANG J, CHEN X, XIE J M, YANG W W, CHEN D L. Effect of aluminum on microstructure and property of Cu–Ni–Si alloys [J]. Materials Science and Engineering A, 2013, 572: 65–74.

[12] LI San-hua, SHEN Lei-nuo, LI Zhou, DONG Qi-yi, XIAO Zhu, XING Yan. Quench sensitivity of Cu–6.5Ni–1Al–1Si–0.15Mg–0.15Ce alloy with super high strength [J]. The Chinese Journal of Nonferrous Metals, 2015, 25(6): 1546–1552. (in Chinese)

[13] ASTM G31–72 (2004). Standard practice for laboratory immersion corrosion testing of materials [S].

[14] SHEN Lei-nuo, LI Zhou, ZHANG Zhe-ming, DONG Qi-yi, XIAO Zhu, LEI Qian, QIU Wen-ting. Effects of silicon and thermomechanical process on microstructure and properties of Cu–10Ni–3Al–0.8Si alloy [J]. Materials and Design, 2014, 62: 265–270.

[15] MAHMOUD S S. Electrochemical studies of pitting corrosion of Cu–Fe alloy in sodium chloride solutions [J]. Journal of Alloys and Compound, 2008, 457: 587–592.

[16] TAIT W S. An introduction to electrochemical corrosion testing for practicing engineers and scientists [M]. Racine Wisconsin: Pair O Docs Publications, 1994.

[17] XIAO Zhu, LI Zhou, ZHU An-yin, ZHAO Yu-yuan, CHEN Jing-lin, ZHU Yun-tian. Surface characterization and corrosion behavior of a novel gold-imitation copper alloy with high tarnish resistance in salt spray environment [J]. Corrosion Science, 2013, 76: 42–51.

[18] AWAD N K, ASHOUR E A, FOUADA A S, ALLAM N K. Effect of alloying elements on the electrochemical behavior of Cu–Ni–Zn ternary system in sulfide-polluted saltwater [J]. Applied Surface Science, 2014, 307: 621–630.

[19] BADWAY W A, ISMAIL K M, FATHI A M. Effect of Ni content on the corrosion behavior of Cu–Ni alloys in neutral chloride solutions [J]. Electrochimica Acta, 2005, 50: 3603–3608.

- [20] KUO H H, WANG W H, HSU Y F, HUANG C A. The corrosion behavior of Cu–Al and Cu–Al–Be shape-memory alloys in 0.5 M H<sub>2</sub>SO<sub>4</sub> solution [J]. Corrosion Science, 2006, 48: 4352–4364.
- [21] SYRETT B C. Erosion-corrosion of copper-nickel alloys in sea water and other aqueous environments—A literature review [J]. Corrosion, 1976, 32(6): 242–252.
- [22] HODGKIESS T, VASSILIOU G. Complexities in the erosion corrosion of copper–nickel alloys in saline water [J]. Desalination, 2005, 183: 235–247.
- [23] SHEN Lei-nuo, LI Zhou, DONG Qi-yi, XIAO Zhu, LI Si, LEI Qian. Microstructure evolution and quench sensitivity of Cu–10Ni–3Al–0.8Si alloy during isothermal treatment [J]. Journal of Materials Research, 2015, 30(5): 736–744.
- [24] SHEN Lei-nuo, LI Zhou, ZHAO Yu-yuan, WANG Yang, DONG Qi-yi, WANG Meng-ying. Phase transformation behavior of Cu–10Ni–3Al–0.8Si alloy [J]. Materials Chemistry and Physics, 2016, 173: 421–428.

## 新型超高强 Cu–Ni–Al–Si 合金在 3.5% NaCl 溶液中的腐蚀行为

朱家俊<sup>1,2</sup>, 黎三华<sup>3</sup>, 申镭诺<sup>3</sup>, 杨武霖<sup>1,2</sup>, 李周<sup>3</sup>

1. 湖南大学 材料科学与工程学院, 长沙 410082;
2. 湖南大学 湖南省喷射沉积技术及应用重点实验室, 长沙 410082;
3. 中南大学 材料科学与工程学院, 长沙 410083

**摘要:** 设计并制备了一种新型超高强 Cu–6.5Ni–1Al–1Si–0.15Mg–0.15Ce 合金, 采用扫描电镜观察、透射电镜观察、光电子能谱分析等手段研究该合金在 3.5%NaCl 溶液中的腐蚀行为。合金经固溶、冷轧 80%并在 450 °C 时效 1 h 后具有最佳的综合性能, 其硬度为 HV 314, 电导率为 19.4%IACS, 抗拉强度为 1017 MPa, 年平均腐蚀速率为 0.028 mm/a。腐蚀初期合金表面形成了氧化腐蚀产物和氯化腐蚀产物, 随着腐蚀时间延长形成了氢氧化物腐蚀产物。合金具有超高的强度、优良的电导率和耐腐蚀性能是由于 Ni<sub>2</sub>Si 能够抑制晶界处粗大 NiAl 相的析出, 并能抑制合金的脱 Ni 腐蚀。

**关键词:** Cu–Ni–Al–Si 合金; Ni<sub>2</sub>Si 析出相; 腐蚀行为; 年平均腐蚀速率; 腐蚀产物

(Edited by Xiang-qun LI)